Available online at www.sciencedirect.com
ScienceDirect
International Journal of Multiphase Flow 32 (2006) 935–956
International Journal of Multiphase Flow
www.elsevier.com/locate/ijmulflow

Adaptive collision meshing and satellite droplet formation in spray simulations

Shuhai Hou [a], David P. Schmidt [b,*]

[a] Caterpillar Inc., Peoria, IL 61656, USA
[b] Department of Mechanical and Industrial Engineering, University of Massachusetts, Engineering Lab Room 219, 160 Governors Dr., Amherst, MA 01003, USA

Received 11 March 2005; received in revised form 8 February 2006

Abstract

Improved numerical methods and physical models have been applied to droplet collision modeling. Numerically, an adaptive collision mesh method is developed to calculate collision rate. This method produces a collision mesh that is independent of the gas phase mesh and adaptively refined according to local parcel number density. An existing model describing the satellite droplet formation during the collision process is improved to reflect the experimental findings that the satellite droplets are much smaller than the parent droplets. The adaptive collision mesh and the improved satellite model have been used to simulate three impinging spray experiments. The model was able to qualitatively predict the occurrence of small satellite drops and bi-modal post-collision drop size distributions. The effect of the collision mesh and the satellite droplet model on a high-speed non-evaporating diesel spray is also assessed.

Keywords: Droplet collision; Collision mesh; Collision outcome

1. Introduction

Droplet collision occurs frequently in dense sprays. The exact importance of collision in determining the droplet size is unknown, but many investigators have found its contribution to be very significant. Gavaises et al. (1996) found large changes in both droplet size and velocity as a consequence of collision. MacInnes and Bracco (1991) noted collision rates of approximately 10^8 per cubic centimeter per micro-second in diesel spray calculations. Since collisions always change the velocity, and often the size of the droplets, only a few collisions during a droplet's lifetime are required to completely change its behavior. Droplet collision has proven difficult to model, however. The problems can be divided into two categories: numerical and physical. The numerical problems are a consequence of mathematical assumptions and limited computational resources. The physical

* Corresponding author. Tel.: +1 413 545 1393; fax: +1 413 545 1027.
E-mail address: Schmidt@ecs.umass.edu (D.P. Schmidt).

0301-9322/$ - see front matter © 2006 Elsevier Ltd. All rights reserved.
doi:10.1016/j.ijmultiphaseflow.2006.02.013

problems result from uncertainty about the mechanisms of collision. Numerical problems generally affect the prediction of the incidence of collision, while physical uncertainties cause errors in the outcomes of collision.

The general approach of Monte-Carlo sampling of droplets is widely used for spray modeling, since it allows a statistical subset of the droplets to be tracked. The tracked droplets, known as parcels, represent numerous droplets from the larger population. This approach is effective for capturing the multidimensional nature of the spray equation (Amsden et al., 1989). However, since only a subset of the actual droplets is tracked, a stochastic approach to collision is required. O'Rourke astutely recognized this and implemented a probability-based collision algorithm. The number density of the droplets is inferred from the locations of parcels, as derived by O'Rourke (1981).

The disadvantage of O'Rourke's technique is that it is computationally inefficient. The cost of the collision calculation goes up rapidly, with the number of parcels squared. This cost discourages computationalists from employing a sufficient number of parcels. Schmidt and Rutland (2000) used the NTC (No Time Counter) method to produce an algorithm that has a linear cost. Both methods are cell-based. Like O'Rourke's collision algorithm, the NTC algorithm is first-order accurate in time and second-order accurate in space. Unlike O'Rourke's collision algorithm, in which all the possible collision pairs are considered, the NTC algorithm only considers a randomly chosen subset of candidate pairs after scaling up the collision probability by the estimated maximum probability, reducing the computational cost. The technique was validated using analytical solutions for collision incidence. The practical significance of the increased efficiency is that one can use a 100,000 parcels and not notice the cost of the collision calculation. Using such large numbers of parcels helps avoid statistical problems and provides a smoother representation of the spray.

Numerical problems with collision have been noticed by several authors. Hieber (2001), Nordin (2000), and Aneja and Abraham (1998) noted that collision rate predictions are traditionally very grid sensitive. Schmidt and Rutland (2000) confirmed this observation, and suggested that the problem lay in the use of the gas phase mesh for calculating number density. This widely used approach of relying on a mesh, established by O'Rourke (1981), is sound when the droplet density variation is well-resolved. In fact, similar techniques are used very successfully in the molecular gas dynamics community for particle collisions (Bird, 1989). However, in sprays, the maximum gas phase mesh resolution is limited by numerical and physical factors (Abraham, 1997). The mesh is generally too coarse to resolve the sharp gradients of number density, especially near the injector orifices. Schmidt and Rutland (2000) showed that collision calculations could be 100% in error when under-resolved, even with a second-order spatial approach. Schmidt and Rutland (2001) and Aneja and Abraham (1998) showed that these errors could cause large errors in droplet sizes.

Grid dependency is one consequence of inadequate numerical methods. Grid dependency due to collision is particularly severe when using a Cartesian mesh, as shown in Fig. 1. The computed spray shape can be turned into a "four-leafed clover" by the grid dependency. Since only parcels located in the same cell are allowed to collide, and the incidence of collision is proportional to the relative velocity between the pair of parcels, the parcels whose trajectories are orthogonal are most likely to collide because they have the greatest relative velocity. Parcels very close to each other, but in different cells, do not collide. In addressing the above shortcomings, Schmidt and Rutland (2000) took advantage of the fact that droplet collisions need not be directly dependent on the gas phase mesh. They proposed a method for creating a collision mesh, independent of the gas phase. An example is shown in Fig. 2. The collision mesh was based on a polar coordinate system aligned with the injector axis. The mesh would automatically form around an injection with any orientation. The angular orientation was chosen randomly every time step to produce a stochastic mesh. This method significantly improved spatial resolution and reduced grid dependency. It was successfully applied to spray bomb and engine simulations. However, this method is only applicable for a single spray because for multiple orifice nozzle sprays there is no single injection axis.

The previously mentioned problems are all numerical and tend to manifest themselves in the prediction of the incidence of collision. Once the numerical problems are resolved, the next step is to address the physics of the problem: what happens as a consequence of collision? Historically, collision outcomes for spray models were based on the work of Brazier-Smith et al. (1971). They conducted experiments on drop collision for water under atmospheric conditions. It was found that permanent coalescence always occurred for head-on collisions. For a fixed collision Weber number the collision resulted in permanent coalescence and coalescence followed by separation with increasing impact parameter. They also proposed a correlation to demarcate the two

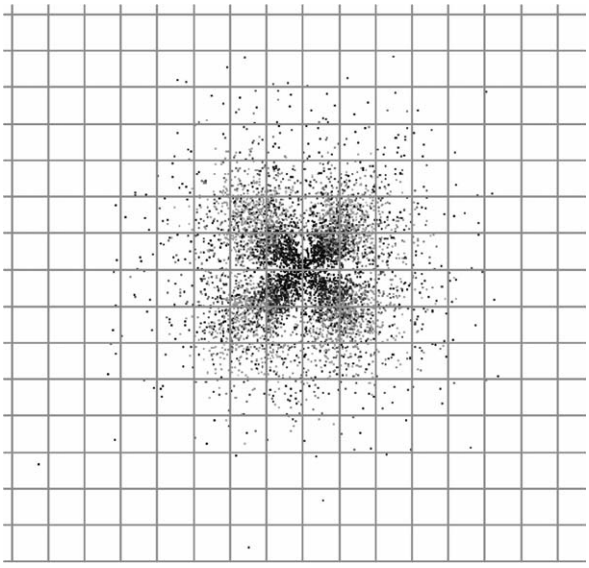

Fig. 1. A nominally axi-symmetric solid-cone spray directed towards the viewer. Mesh dependency causes an unrealistic spray shape.

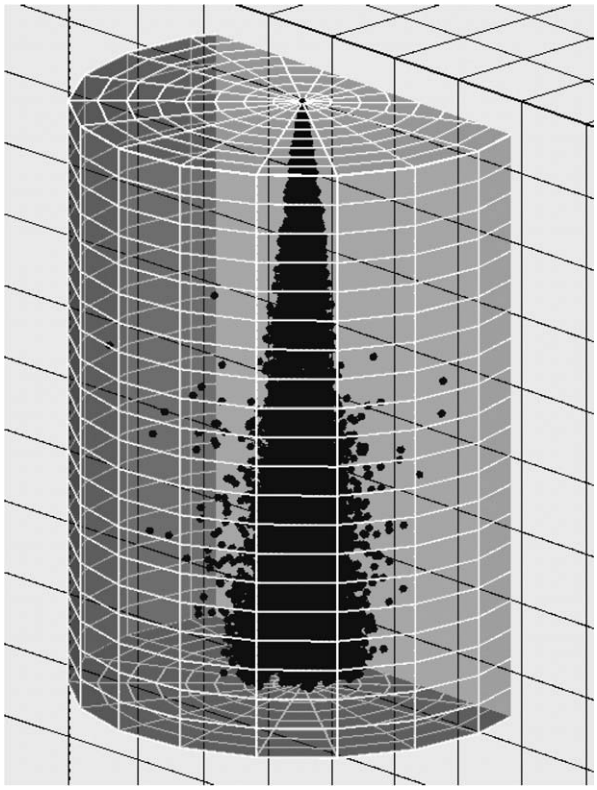

Fig. 2. A cylindrical collision mesh surrounding a computed spray. The background Cartesian mesh is the gas phase mesh.

outcomes, which is still widely used in diesel spray modeling. However it is questionable to extend the results for water drop collision under atmospheric conditions to diesel sprays, since the conditions in the two

phenomena are significantly different. Jiang et al. (1992) performed extensive quantitative experiments on the collision behavior of hydrocarbon droplets. They found the collision outcomes for hydrocarbon droplets were more complex than that for water droplets. For head-on collisions, the outcome was far from being monotonic, i.e., collision could result in permanent coalescence after minor deformation (low-speed coalescence), bouncing, permanent coalescence after large deformation, and temporary coalescence followed by separation with or without the production of satellite droplets. Qian and Law (1997) qualitatively extended the results to include the effects of gas pressure, viscosity, molecular weight and molecular structure. It was shown that collision outcomes are far too complex to be parameterized only by collision Weber number, impact parameter, and size ratio, an observation confirmed by other investigators. Transition from bouncing to permanent coalescence was found to strongly depend on the gas properties, since whether the droplets bounce or not depends on the gas build-up between them. They concluded that the difference in the collision behavior of water and hydrocarbon droplets could be attributed to their different properties. By changing the gas properties, water droplets could exhibit the same outcomes as that of hydrocarbon droplets. Thus the different droplet collision outcomes of water and hydrocarbon were unified. These experimental studies provide us with significant insights into the collision behavior of hydrocarbon droplets, but it is still a challenging task to quantitatively describe the major effects, and the validity to directly extrapolate the results to the diesel spray modeling is still an open question. Considerably more work is needed in modeling collision outcomes in diesel sprays.

To take advantage of the new experimental findings, Post and Abraham (2002b) used published correlations to incorporate the new collision outcomes into multidimensional diesel spray calculations. Low-speed coalescence was omitted because it is of no practical interest. Bouncing was accounted for with the correlation from Estrade et al. (1999), reflexive separation from Ashgriz and Poo (1990), stretching separation and permanent coalescence from Brazier-Smith et al. (1971). To reproduce the experimentally observed increased bouncing at elevated gas pressure, Post et al. included an extra term in the correlation for bouncing to take into account the gas density. They ran two-dimensional simulations using O'Rourke's method of calculating collision incidence, and found that, when compared to O'Rourke's model, the hydrocarbon-based outcomes produced much smaller drops.

Stretching and reflexive separation are often accompanied by ligament stretching and satellite droplet formation, which can be a frequent event (Hung, 1998; Ashgriz and Poo, 1990; Jiang et al., 1992; Qian and Law, 1997; Brenn et al., 1997), and can play a significant role in determining the spray characteristics. They can be particularly significant in vaporizing sprays since smaller droplets enhance the vaporization considerably. The literature on modeling satellite formation is sparse, and its effects have often been neglected in diesel spray modeling. Georjon and Reitz (1999) proposed a satellite droplet model based on the Rayleigh linear jet breakup theory. The physical basis of this model, though referred to as "shattering", actually resembles the process of ligament elongation and breakup following temporary coalescence. In the model it is assumed that the two collided droplets are transformed into an initially spherical drop. Then the sphere stretches into a cylinder whose radius evolves based on energy conservation. As the cylinder elongates, capillary disturbances can grow and break up the cylinder into droplets of equal size. One limitation of this model is that it predicts all of the product droplets are the same size, which is contrary to the experimental observations that the satellite droplets are much smaller than the parent droplets. As a consequence, the small drops measured in the experiments by Hung (1998) were missed in Georjon and Reitz's simulation with their model.

To satisfactorily model collision, both the numerical techniques and the model physics must be accurate. The current work proposes a new numerical method for calculating the incidence of collision using a general adaptive-mesh method. The modeling physics take advantage of the advances of Post and Abraham (2002b) and Georjon and Reitz (1999). The satellite droplet model is improved in order to predict non-uniform droplet size after collision. The goal of this effort is to accurately simulate collision using both advanced numerical techniques and physics.

2. Adaptive collision mesh

Collision cells are used for grouping parcels, so that kinetic theory can be used to predict collision rates. Historically, the gas phase mesh has been used for this grouping. If a separate collision mesh is used, one can optimize the resolution to balance the requirements of small cells for high spatial resolution and larger

cells for larger sample size and better statistical resolution. Further, the collision mesh should be stochastic. A stochastic mesh accomplishes the common-sense goal of collision modeling: that parcels that are near each other should be allowed a chance to collide. With a deterministic collision mesh, parcels which are quite close may repeatedly find themselves in differing cells, and this prevented from colliding. This problem typically occurs when injection is oriented with one of the cardinal directions on a regular mesh. In contrast, in a stochastic mesh, parcels that are close to each other are usually going to be found in the same cell. Parcels that are further apart are less likely to be in the same cell.

Mathematically, the collision mesh is intended to provide a parcel with a set of potential collision partners that are spatially unbiased, e.g. on average, the potential collision partners lie in a volume that is centered on the parcel of interest. First, consider the collision frequency per unit volume between two droplets with properties 1 and 2, as defined by O'Rourke and reviewed later by MacInnes and Bracco (1991), given by Eq. (1)

$$v_{ab} = f_1 f_2 \pi (r_1 + r_2)^2 |\vec{u}_1 - \vec{u}_2| \, \mathrm{d}\vec{u}_1 \, \mathrm{d}r_1 \, \mathrm{d}\vec{u}_2 \, \mathrm{d}r_2 \tag{1}$$

The value of $\vec{u}$ corresponds to the velocity of droplet 1 or 2, depending on the subscript. Similarly, r is the radius and f is the number distribution function in the seven-dimensional space defined by position, velocity, and radius. This approach to collision assumes locality, as defined by Subramaniam (2001). Hence, the collision frequency at a point of interest, $\vec{X}$, depends on the number density of droplets and their corresponding properties at that point. However, the Monte-Carlo approach to droplet collision requires a reasonable sample size. In order to collect a sufficient sample size, parcels in the vicinity of $\vec{X}$ are used. Considering candidates for collision from a small volume that is symmetric around $\vec{X}$ will provide a second-order accurate, unbiased estimation of number density and similar quantities which are used for collision (Bartlett, 1963).

In the present work, a three-dimensional mesh is created at every time step and refined where the spray is dense. The adaptive meshing algorithm is based on the following steps:

1. Generate a Cartesian reference frame with a completely random orientation. The collision mesh will be aligned with this randomly oriented orthogonal coordinate system. This step is important to suppress the artifacts caused by a static Cartesian mesh. The randomness ensures that the collision mesh will be entirely different at every time step.
2. Create a cube oriented with the axes from the previous step and encompassing all the parcels in the computational domain. By using a cube instead of a hexahedron, large cell aspect ratios are avoided. If long, slender cells are for some reason desirable, only a trivial change to the algorithm is required.
3. Check if the number of parcels in the cube is below the maximum allowed number. If so, the mesh is completed. If not, continue to the next step. The maximum allowed number is used to control the spatial resolution of the mesh, and at the same time to make sure that sufficient number of parcels are in the cells. This number is called the "partitioning criterion number".
4. Halve the cube in the x, y and z directions to make eight smaller cubes.
5. Check each smaller cube to see if the number of parcels in it is below the partitioning criterion number. If so for all the interior cubes, the mesh refinement is completed. If not, repeat steps 4 and 5 for all the cubes in which the number of parcels exceeds the partitioning criterion number.

This approach results in a mesh that is finer where the spray is dense and coarser where the spray is sparse. Fig. 3 shows one picture of the adaptive collision mesh. It can be seen that the collision cells are smaller in the denser areas. The rectangular cells that comprise the mesh are not oriented with any of the sprays; the orientation of the mesh is randomly chosen every time step. Fig. 4 shows its effectiveness in avoiding the grid dependency caused by a Cartesian mesh using as the collision mesh. Due to the stochastic nature of the mesh, it is entirely different every time step. Grid artifacts, which appear when the parcels are artificially forbidden to collide with near-neighbors, are prevented. Instead, the stochastic grouping means that the parcels that are close to each other are likely to end up in the same collision cell during most time steps. This stochastic meshing removes one of the objections to Monte-Carlo droplet collision algorithms: that parcels which are quite close to each other may fall into different cells and be prevented from colliding. Another value of this approach

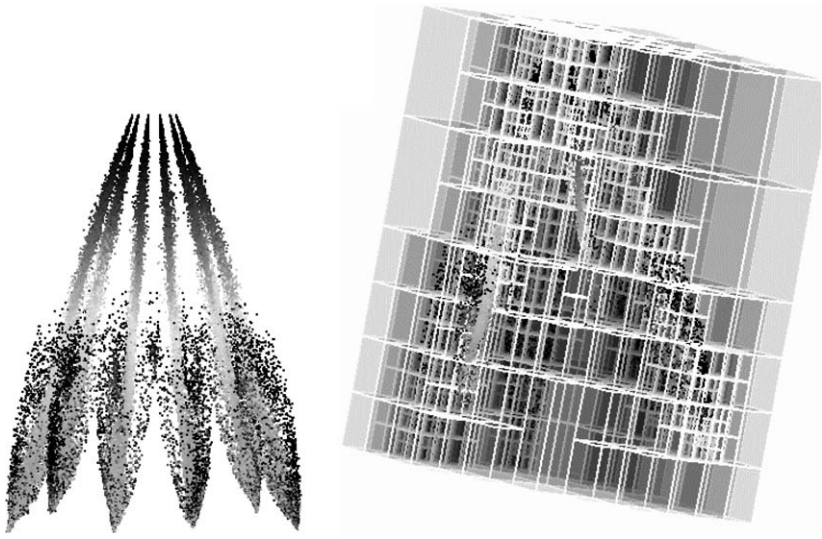

Fig. 3. Sprays from a six-hole injector (left) and the adaptive mesh (right) that is formed around the sprays. Part of the sprays and mesh are cut away for clarity.

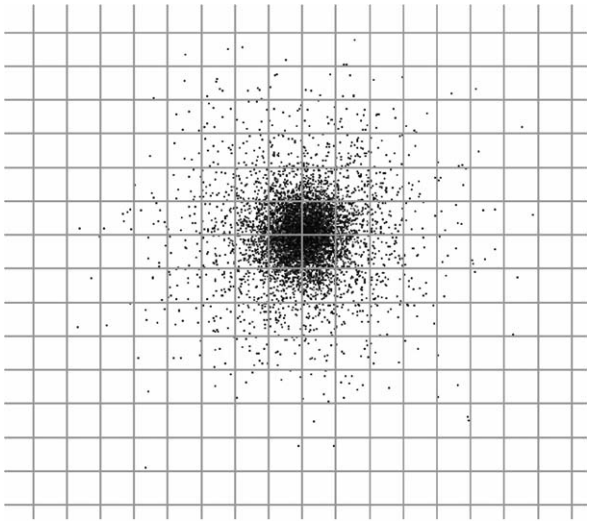

Fig. 4. Predicted shape of the spray using the adaptive collision mesh. Conditions are the same as in Fig. 1.

is that the collision mesh is not tied to any one geometric configuration. It can be used for any number of sprays in any orientation. The typical CPU cost of calculating collisions in this manner is a trivial amount of the total simulation time. Bird's original implementation of the NTC method, which requires an ensemble average of the number density for the cells, is not easily coupled to an adaptive mesh. As in Garcia (2000) and Schmidt and Rutland (2000), a variant of the NTC method that uses instantaneous statistics is employed.

One limitation of the current approach is that parts of the collision mesh may be outside the computational domain. To some degree, this may not be a problem. If part of the collision mesh is outside of the computational domain, no parcels will be present in that part of the collision mesh. However, if collisions near a boundary are of primary concern, it may be necessary to calculate the true volume of collision cells that intersect the computation domain.

3. Satellite droplet model

The model of Georjon and Reitz (1999) was constrained by computational cost. Because of the N-squared cost of O'Rourke's collision algorithm, Georjon and Reitz's collision model was designed to avoid creating large numbers of new parcels. As a consequence, the product of satellite breakup was a parcel containing droplets of uniform size. The speed of the NTC algorithm permits the present work to represent the products of satellite droplet formation with greater fidelity. In the present work, a modification is made to the model by Georjon and Reitz to allow the relatively small child drops to be differentiated from the larger parent drops. Further, the Georjon and Reitz model is simplified; based on the analysis of Post and Abraham, the process of integrating ordinary differential equations representing capillary formation is skipped in favor of a closed-form approximate solution.

It is phenomenologically assumed that the volume that forms the child drops is the portion of the two parent droplets that would be in actual contact upon collision. As illustrated in Fig. 5, only the shaded volume, instead of the total volume of the two parent droplets, is considered to undergo breakup. It is obvious that the volume that is to stretch and form the satellite droplets depends on the angle, θ, and the drop radii. The greater the sine of the angle, the smaller the volume of the stretching ligament, and hence the smaller the satellite droplets. It is expected that this model modification can predict satellite droplets with size smaller than the parent droplets.

The simplification made by Post and Abraham (2002b) to Georjon and Reitz's model (1999) at high Weber number limit is used in the calculations to limit computational cost. The satellite droplet radius is given by

$$r = \frac{1.89R_S}{\sqrt{(13.86\alpha)^{4/7}We^{2/7}(1+\Delta^{-3})^{2/21}+1}} \tag{2}$$

where R_S is the nominal radius of the initial sphere, We is the collision Weber number defined as $\rho_d W^2 R_{small}/\sigma$, Δ is the droplet size ratio defined as R_{small}/R_{large}, and α is a geometrical coefficient that measures the initial sphere-to-cylinder transformation velocity. A value of 0.7 for α is used in this work. Once the satellite droplet radius has been determined, the number of drops can be calculated from conservation of mass. The mass comprising the satellite droplets is shown in Fig. 5. The angle θ is determined stochastically, following O'Rourke. There is significant inconsistency in the literature regarding the lower limit of collision Weber number above which satellite droplets will be formed (see Orme, 1997 for a review). A value of 40 is chosen in this work to achieve better agreement with the experimental data.

In light of the recent experimental findings for hydrocarbon droplets, the composite model employed by Post and Abraham (2002b) is used to predict collision outcome. Four collision outcomes are considered

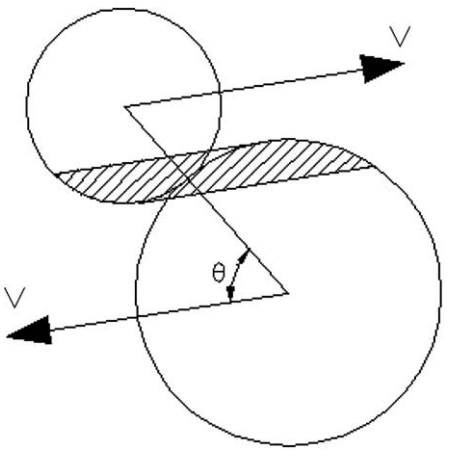

Fig. 5. Illustration of the volume considered for satellite droplet formation.

including bouncing, permanent coalescence, stretching separation and reflexive separation. Satellite droplet formation is considered in the event of stretching separation.

The computations in this work have been performed on a multidimensional spray simulation code MOSES (MOdifiable Source Engine Simulation), which employs an Eulerian gas and Lagrangian particle tracking approach. For a detailed discussion of the numerical accuracy of this scheme, the reader is referred to Are et al. (2005). The gas phase Navier–Stokes solver uses a finite difference method with a uniform, regular block-structured, co-located mesh. The convection terms can be treated with either first-, second-, or third-order schemes. For simulations where the surrounding air was presumed to have little influence (the first three simulations reported below), first-order upwinding was used. For simulating the experiment of Baik et al., where aerodynamic effects were known to be significant, third-order upwinding was used. With minor modifications, the PISO (Pressure Implicit with Splitting of Operators) method is used for the velocity–pressure coupling in solving the gas phase transport equations (Issa, 1985). Turbulence is represented by the RNG k–ε model. Are et al. (2005) have shown that the basic two-way coupling and Navier–Stokes solver is second-order accurate.

In simulating the spray impingement experiments by Hung (1998) and Brenn et al. (1997), no breakup models are used since the droplet Weber number is low enough for the droplet to remain stable. The TAB model (O'Rourke and Amsden, 1987) is employed in the simulation of the experiment by Arai and Saito (1999), since the injected droplet Weber number was slightly greater than 6. In the simulation of the high-speed non-evaporating spray by Baik et al. (2003), the WAVE model (Reitz, 1987) is used to describe both the primary atomization and droplet secondary breakup. The model by Zhou and Leschziner (1991) is employed to describe droplet dispersion due to turbulence. For the simulation of the three spray impingement experiments, the mesh resolution was $2 \times 2 \times 2$ mm. For the high-speed non-evaporating spray experiment, the mesh resolution was $1 \times 1 \times 2$ mm. Between 160,000 and 300,000 parcels were used in the simulations. The collision rate is calculated using the NTC algorithm with the adaptive Cartesian mesh.

4. Testing and validation

The spray impingement experiments by Hung (1998), Brenn et al. (1997), and Arai and Saito (1999) were chosen to evaluate the collision mesh and satellite droplet model. In these experiments, two streams of liquid droplets intersected at different angles at room temperature and pressure. Qualitative and quantitative descriptions of the collision behavior between the two sprays were provided in the experiments. The droplet Weber number was controlled to be low enough to have no or very weak breakup. By creating collisions between these well-characterized streams of liquid droplets, these experiments are ideal for assessing collision models, since the collision process is nearly isolated from other complex spray physics, which would not be possible in normal diesel spray experiments.

The performance of the collision mesh on a high-speed non-evaporating spray is assessed using the experiment by Baik et al. (2003). The effect of the satellite droplet model on the prediction of spray characteristics is also explored using this experiment.

The numerical quality of the solutions was checked, in order to verify that the calculations were mesh independent. The adaptive meshing scheme was tested with several different values of the partitioning criterion. For a fixed number of parcels, the smaller the value of the partitioning criterion, the finer the resulting mesh. For example, a value of 80 produced a mesh where 80% of the cells were less than 0.5 mm in size. By decreasing the value of this criterion, one can force the mesh to become increasingly fine. The effect of this mesh refinement via reduced partitioning criteria is presented in Fig. 6. The smallest collision cells in each of the four cases had volumes of 7.37×10^{-6}, 6.32×10^{-6}, 9.95×10^{-7}, 1.18×10^{-7} mm^3, respectively. Even given this apparently small dynamic range of mesh sizes, Fig. 6 shows that the drop size distribution converges rapidly.

Reducing the partitioning criterion is a way to achieve higher resolution with little cost. However, this refinement cannot continue without limit. Post and Abraham (2002a) have explained the need for maintaining an adequate number of parcels per collision cell in collision calculations. The literature, however, offers no rigorous lower bound to the partitioning criterion. Many researchers employ Bird's use of ensemble averaged number density, which is not appropriate for an adaptive mesh. The variant of the NTC method described by Garcia (2000) is used here. As an example, Alexander and Garcia (1997) used 1000 particles per cell for gas

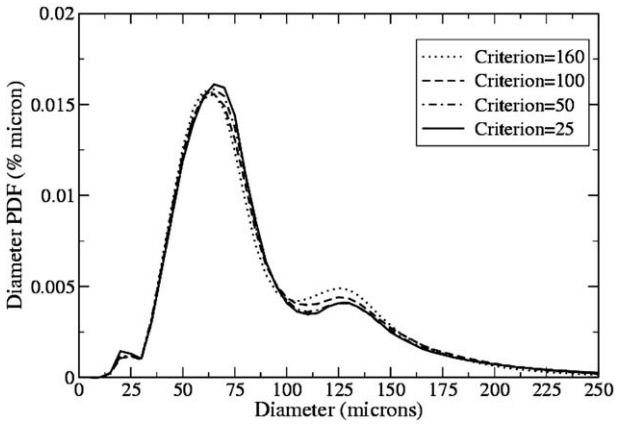

Fig. 6. Predicted size distribution for an intersecting spray simulation with varying partitioning criterion. The corresponding mesh resolutions are given in the text.

dynamics simulations which would correspond to a partitioning criterion of 8000 for a three-dimensional adaptive mesh. Park et al. (2002) used at least 100 parcels per cell in their NTC calculations.

To investigate the lower bound, a spatially uniform test case of Schmidt and Rutland (2000) is used, because it permits an analytical solution. With an exact solution, the numerical error is of a calculation is known exactly. This test problem consists of N droplets in a three-dimensional volume $\mathcal{V}$ with sizes randomly chosen from 0 to $r_{\max}$. The z-component of velocity is randomly chosen to be from 0 to $u_{\max}$, and the other two components of velocity are zero. Each parcel is chosen to represent between zero and $q_{\max}$ droplets. Each of these random quantities is based on a uniform random deviate. The only difference between the present test and Schmidt and Rutland's uniform test case is that here the positions of the particles are randomly chosen in a three-dimensional rectangle with unit volume. The volume is divided into varying numbers of rectangular cells of equal volume, which varies the average number of parcels per cell. The expected number of collisions over a short time interval, Δt, was calculated from the integral of the collision probability over the size and velocity space of each possible partner. The integral is given below:

$$M_{\text{coll}} = \frac{N^2 \Delta t}{2\mathcal{V}} \int_0^{r_{\max}} \int_0^{r_{\max}} \int_0^{u_{\max}} \int_0^{u_{\max}} f_u(u_1) f_u(u_2) f_r(r_1) f_r(r_2) |u_1 - u_2| \pi (r_1 + r_2)^2 \, \mathrm{d}u_1 \, \mathrm{d}u_2 \, \mathrm{d}r_1 \, \mathrm{d}r_2 \tag{3}$$

The functions f represent the probability distribution functions, which in this case are simply uniform distributions in all dimensions. The integrand corresponds to Eq. (1). The evaluation of this integral gives the following expected number of collision:

$$M_{\text{coll}} = \frac{7\pi \Delta t u_{\max} r_{\max}^2 N^2}{36\mathcal{V}} \tag{4}$$

The results of the test using 25,000 parcels are shown in Fig. 7. The values used for the maximum radius, maximum velocity, and the time interval are 50 μm, 100 m/s, and 5 ms, respectively. The error is quantified as a percentage difference between the number of collisions predicted by the NTC method and Eq. (4). The sign of the error indicates whether the predicted number of collisions exceeded (positive error) or were less than (negative error) the mean expected number of collisions. Note that there is no trend to the error and that an average of five parcels per cell is clearly sufficient to accurately predict the incidence of collision. A mathematical derivation showing the independence of the predictions on number of parcels per cell is given in Appendix A. According to the derivation, so long as the partitioning criterion is greater than or equal to two, the average prediction of collision should be adequate. Thus the average number of parcels per cell can be less than unity. This is an astonishingly low number of parcels, but the analytical and empirical results clearly show that the average number of parcels per cell can be far lower than has been used in the past. In the present work with a moderate value of the partitioning criterion (a setting of 80), 2.5% of the cells contained fewer than five parcels.

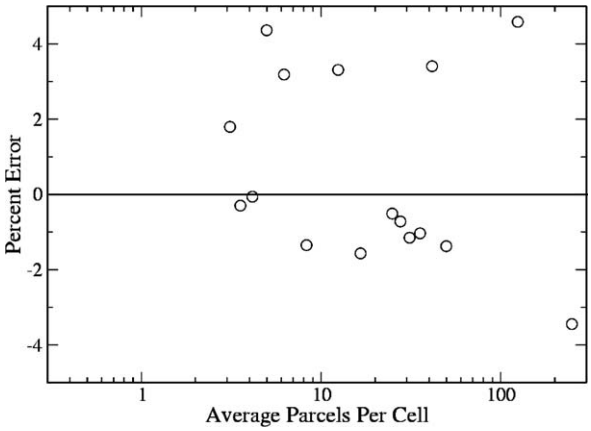

Fig. 7. Results of a spatially uniform test designed to check sensitivity of the predicted number of collisions on the numbers of parcels per collision cell.

Spatial accuracy will benefit from the smaller cells. Previous testing by Schmidt and Rutland (2000) shows that the NTC method converges with second-order spatial accuracy and first-order temporal accuracy when sufficiently large numbers of parcels are used. In the current work, several spray calculations were repeated using half the number of parcels in order to verify that the results were not affected.

4.1. Spray impingement simulation I

In Hung's (1998) experiment two quasi-monodisperse streams of droplets intersect to produce a fan of post-collision droplets. The streams are produced through two sapphire plain orifice nozzles with a diameter of 50.8 μm. The nozzles are mounted to allow variable angular orientation in a vertical plane. The injection pressure is 0.689 MPa, at which the droplets are produced by Rayleigh breakup with approximately twice the nozzle diameter. Data are gathered for intersecting angles of 10°, 15° and 20°. The fluid used is Mineral Spirit Rule 66. At standard temperature and pressure, the fluid has a density of 776 kg/m^3, a surface tension coefficient of 0.0237 N/m, and a viscosity of 0.00336 kg/(m s).

A 1-D Phase Doppler Particle Analyzer (PDPA) and stop-action micro-photography were employed for measurement in both the individual droplet streams and the collision area. For individual droplet streams, it was shown that the droplet Weber number ranged from 0.89 to 6.9, and 0.48 to 3.48 for nozzles 1 and 2, respectively. So it would be safe to assume that the droplets were aerodynamically stable before collision. In addition, stop-action micro-photography did not reveal any droplets undergoing aerodynamic breakup prior to the intersecting point. The measurement volume of the PDPA was placed 2 cm directly below the intersecting point of the two streams.

The droplet size and velocity prior to collision for the individual nozzles follow a Gaussian distribution (Hung, 1998). The means and standard deviations of the injected distributions have been determined by matching the experimental data of droplet size and velocity prior to collision. For nozzle 1, the mean and standard deviation of the droplet size distribution was 131 μm and 22 μm, and the mean and standard deviation of the droplet velocity distribution was 22.9 m/s and 0.53 m/s. For nozzle 2, the mean and standard deviation of the droplet size distribution was 138 μm and 17 μm, and the mean and standard deviation of droplet velocity distribution is 16.2 m/s and 0.4 m/s.

The characteristics of the adaptive collision mesh are presented for the 20° case as an example. Fig. 8 gives an illustration of the collision mesh where the coordinate axes of the gas phase mesh are aligned with the collision mesh for clarity. Normally, at any given time step the collision mesh is given some random orientation. Note that the cubes with lighter sidelines are the gas phase mesh cells, which are much larger than the collision mesh cells. It is evident that the mesh is finest at the intersecting area.

Figs. 9–11 show the computed droplet size distribution for the intersecting angle of 10°, 15° and 20°, respectively. Compared with the droplet size distribution prior to collision, the droplet size distributions are wider

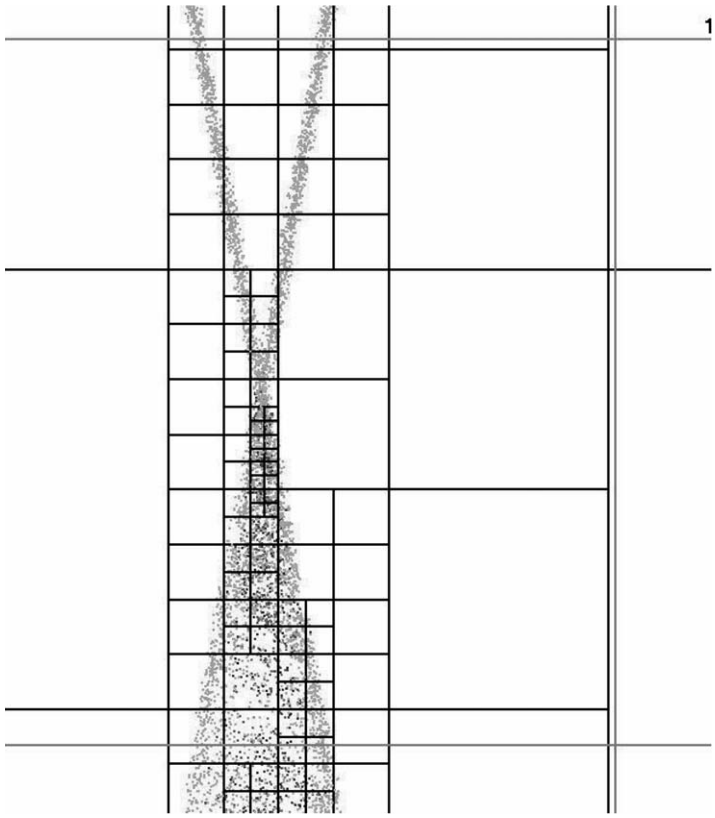

Fig. 8. An illustration of the adaptive collision mesh. For clarity, the collision mesh axes have been aligned with the gas phase mesh axes.

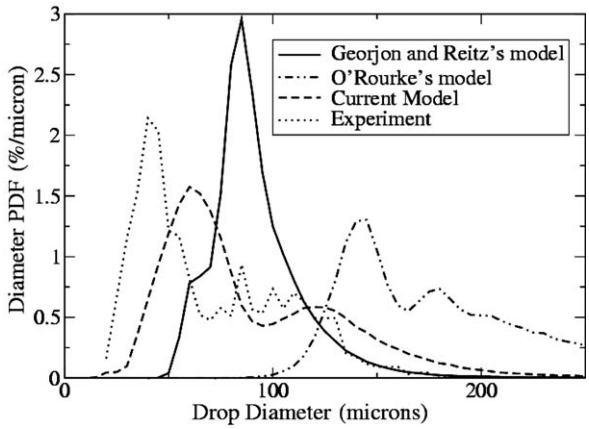

Fig. 9. Droplet size distribution for the intersecting angle of 10°.

and the peaks are smaller after collision. For the intersecting angle of 10° and 15°, the model predicts the bimodal distribution with the peaks shifting to larger values as compared to the measurements. The first peak shows a slight increase as the intersecting angle increases from 10° to 15° as both in the prediction and experiment. As the intersecting angle changes from 15° to 20°, the model predicts an increase of about 10 μm, while the experimental data show an increase of about 20 μm, for the first peak. The model prediction of droplet sizes seems not as sensitive to the intersecting angle as the experimental data.

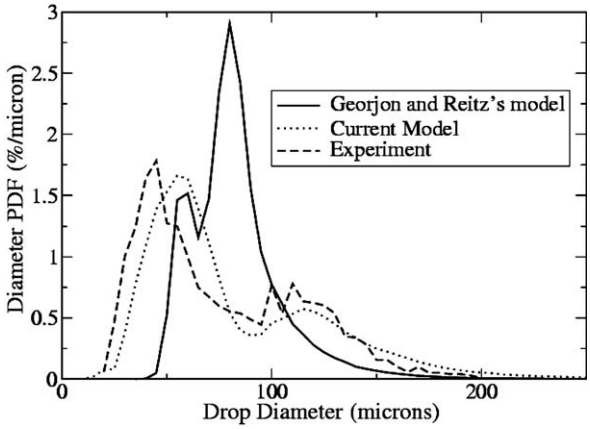

Fig. 10. Droplet size distribution for the intersecting angle of 15°.

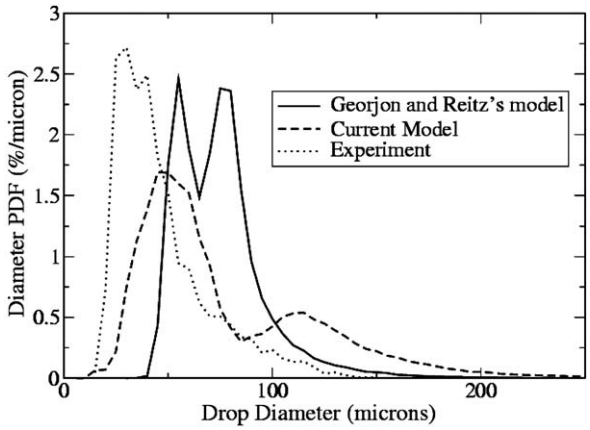

Fig. 11. Droplet size distribution for the intersecting angle of 20°.

One reason for the discrepancy between the prediction and experimental data may be due to the inadequacy of the basic physics assumed for the satellite droplet formation. In the model, the Rayleigh breakup of the regular cylindrical ligament leads to the satellite droplets. Although the photographs by Hung show the ligament stretching can produce small satellite droplets, they also reveal other important mechanisms that are responsible for the production of the satellite droplets. The impact of two droplets can result in a large pancake structure that can be overtaken and hit by fast moving droplets, leading to small droplets. More energetic collision can result in many widely spread ligaments that can breakup into small droplets like the catastrophic aerodynamic breakup. The droplet diameter–velocity correlations shown by Hung (1998) display two distinct groups of droplets, indicating more than one mechanisms are responsible for the production of the small droplets.

Although the predicted droplet sizes are overall larger than the experimental data, it can be seen from the three figures that the values of the lower end of the size distribution agree well with the measurements. This is due to the improvement of the model as described in Fig. 5. Fig. 9 also shows the comparison of the predicted droplet size distribution using Georjon and Reitz's model (with Post and Abraham's analytical closure) and the current improved model for the intersecting angle of 10°. It can be seen that the smallest droplets are not predicted by Georjon and Reitz's model. Their model significantly over-predicts the PDF value at the peak. Although the current model predicts a peak larger than the experiment, the peak is closer to the experimental data than Georjon and Reitz's model. Also shown in Fig. 9 are the results of O'Rourke's outcome model

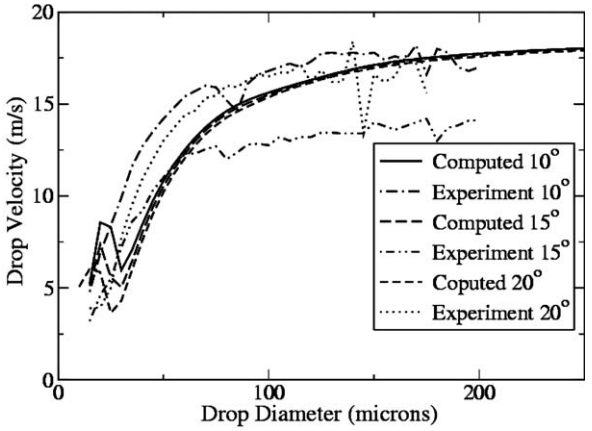

Fig. 12. Droplet velocity for the intersecting angle of 10°, 15°, and 20°.

which is widely used in spray modeling. It is clear that O'Rourke's model only predicts larger droplets than the pre-collision droplets.

Figs. 10 and 11 show the similar comparison for the intersecting angle of 15° and 20°. Again it can be seen that the smallest droplets are predicted only by the current model. The assumption that a reduced amount of mass contained in the stretched ligament between parent drops is responsible for forming the child drops gives rise to the smaller droplets seen in the experiments.

Fig. 12 shows the predicted droplet velocity for the intersecting angle of 10°, 15° and 20°, respectively. The velocity data in the experiment were correlated to the diameter in scattered plots. It would be difficult to directly compare these scattered plots with those obtained in the simulation. So the velocity data in Fig. 12 have been droplet number averaged with a diameter interval of 5 μm. It can be seen that the droplet velocity has a wider range after collision than before the collision. The predicted results agree fairly well with the experimental data. The non-sensitivity of the droplet size prediction to the intersecting angles leads to similar velocity distribution for the three intersecting angles.

4.2. Spray impingement simulation II

Brenn et al. (1997) conducted a similar experiment to Hung but with a different working fluid and larger intersection angles. Two streams of droplet produced by Rayleigh breakup of laminar jets were injected at intersecting angles of 20°, 30°, and 40°. The nominal diameter of the two single-hole nozzles was 20 μm, and the working fluid was propanol-2. At room temperature and pressure, this liquid has a density of 785.4 kg/m^3, a surface tension coefficient of 0.0214 N/m, and a viscosity of 0.002427 kg/(m s). The liquid was injected at a mass flow rate of 0.298 cm^3/min. A one-component Phase Doppler Anemometer was used to measure droplet size and velocity.

The droplet size and velocity distribution prior to collision were not reported by Brenn et al. However, measurement data were recorded for droplet size and velocity distribution in the two main streams at 10 mm, 15 mm and 20 mm directly downstream of the intersecting point. The droplet size and velocity prior to collision appeared to be normally distributed, so a Gaussian distribution was used in the simulations. Following the experimental data, the mean of the droplet size distribution was about 75 μm, and the mean of the droplet velocity distribution was about 11.75 m/s. The standard deviation of the size and velocity distribution were chosen to be 9 μm and 0.2 m/s to give narrow distribution.

The droplet size distributions at 15 mm directly downstream of the intersecting point were calculated and compared with the experimental data. Fig. 13 shows the model prediction and the experimental data for the intersecting angles of 20°, 30°, and 40°, respectively. The model predicts the bi-modal distribution for all of the three intersecting angles. For the intersecting angle of 20°, the model predicts smaller variance and a larger peak than the experimental data. Except for the intersecting angle of 20°, the predicted peaks and variances

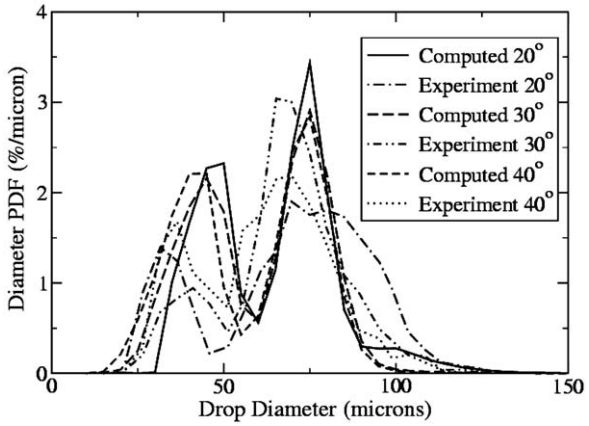

Fig. 13. Droplet size distributions for the intersecting angles of 20°, 30°, and 40° corresponding to Brenn et al. (1997).

agree well with the measurements. It is also noted that the prediction is not very sensitive to the intersecting angle, similar to the simulation of Hung's experiment.

4.3. Spray impingement simulation III

The experiment of Arai and Saito (1999) created an intersection of two transient sprays, unlike the relatively steady, low-speed streams of the two previous experiments. Two sprays from two pintle-type electronic fuel injection nozzles intersected at an angle of $\theta_{imp} = 90°$. The intersecting point was 50 mm downstream the nozzle exit. The hole diameter of the two nozzles was 810 μm, and the injection pressure was 0.25 MPa. The working fluid was ethanol with a density of 789 kg/m^3, a surface tension coefficient of 0.0177 N/m, and a viscosity of 0.001074 kg/(m s) at room temperature and pressure. The SMD of the sprays was measured using a particle analyzer with a laser diffraction technique. The laser beam diameter was 9 mm, and it was located at $L_{tip} = 100$ mm pointing perpendicular to a single spray.

Fig. 14 shows the prediction of SMD at the measurement location. It can be seen that the predicted SMD agrees well with the measurements at the early stage of injection. As injection continues, more and more satellite droplets resulting from collision pass through the measurement location. As seen in the previous simulations, the model tends to over-predict the satellite droplet size. So the difference between the SMD prediction and measurement gets larger as time goes on.

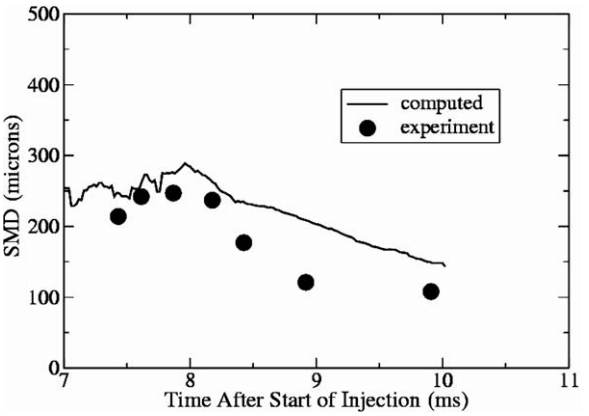

Fig. 14. SMD at the measurement location corresponding to the experiment of Arai and Saito (1999).

4.4. High-speed spray simulation

To assess the capability of the adaptive collision mesh on realistic sprays, the experiments by Baik et al. (2003) on high-speed non-vaporizing sprays in a constant volume chamber and at room temperature were simulated using the adaptive collision mesh. Then the improved satellite droplet model was applied to the same simulation to explore it effect on the prediction of spray characteristics. Three types of single-hole nozzles, with diameter 40, 60, and 80 μm, respectively, were simulated.

The working fluid used was California diesel fuel. At the experimental conditions, it has a density of 841 kg/m^3, a viscosity of 3.36×10^{-3} kg/(m s), and a surface tension coefficient of 0.027 N/m. Experiments were performed in a pressurized constant volume chamber. The ambient gas was Argon and density was 18.7 kg/m^3. The maximum injection pressure was 70–80 MPa. The droplet size of the whole spray was measured by the Light Extinction Technique (LET).

The performance of the collision mesh was checked 0.5 ms after the start of injection. Over 80% of the parcels are located in the collision cells with size less than 0.5 mm. Despite the high resolution of the mesh, over 95.5% of the parcels reside in the collision cells containing more than five parcels. Additional testing and mesh statistics may be found in Hou and Schmidt (2004).

Fig. 15 shows the computed spray tip penetration, and Fig. 16 shows the computed global SMD at the end of injection. It can be seen that both the spray tip penetration and global SMD agree fairly well with the experimental data. Though the sprays emanating from larger holes penetrate faster, there is no significant trend in average drop size. The relative independence of drop size on the orifice diameter suggests the greater importance of downstream physics than primary atomization for determining drop size.

Effects of the adaptive mesh on the predicted spray characteristics are shown in Fig. 17 for the 40-μm nozzle. Calculations were made with O'Rourke's outcome model as well as the composite outcome model. From Fig. 17 it can be seen that the spray tip penetration is not sensitive to the collision meshes and outcome models. This observation is consistent with the findings of Reitz and Diwakar (1987) that penetration is largely dependent on the turbulence diffusivity of the gas phase. Despite predictions of different average drop sizes with different approaches to collision, penetration is not altered.

However the adaptive collision mesh produces persistently larger global SMD than that with the traditional fixed mesh for both outcome models, as shown in Fig. 18. At the immediate start of injection, the difference is imperceptible due to the strong breakup of the injected droplets. As time progresses, large differences in droplet sizes and velocities make the effects of droplet collision much more pronounced. With the adaptive mesh, higher collision incidence, thus higher rate of coalescence, is predicted than with the fixed mesh due to the finer resolution of the adaptive mesh. Note that the gas phase mesh is already fine, so the differences are not very prominent, and seem to be decreasing with time. There are two possible reasons for this behavior: one is that as the spray gets more spread out, the droplet number density decreases. Thus

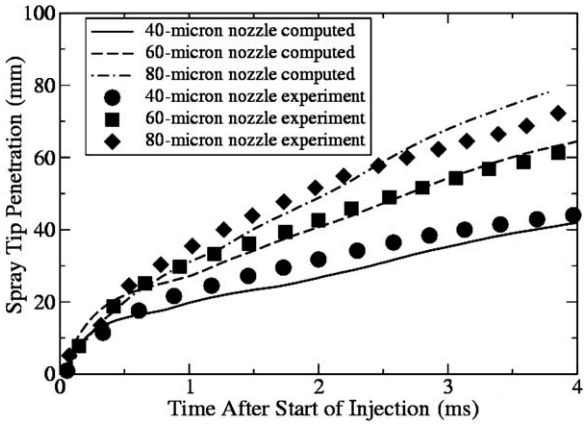

Fig. 15. Spray tip penetration for different nozzles.

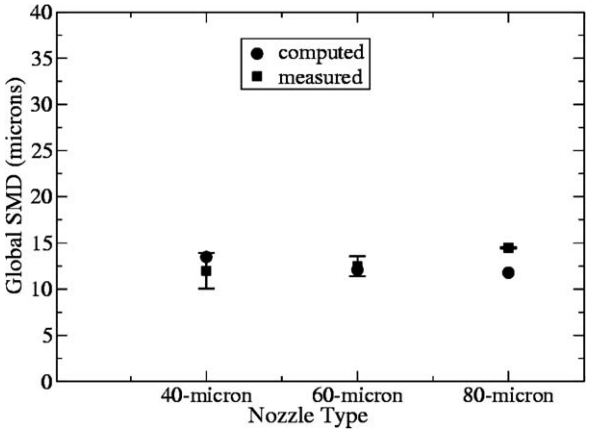

Fig. 16. Simulated and measured global SMD at the end of injection. The error bars show the reported standard deviations from Baik et al.'s data.

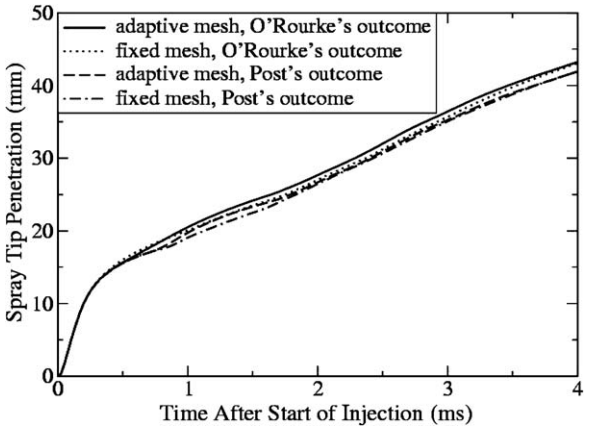

Fig. 17. Effect of the adaptive collision mesh on the predicted spray tip penetration.

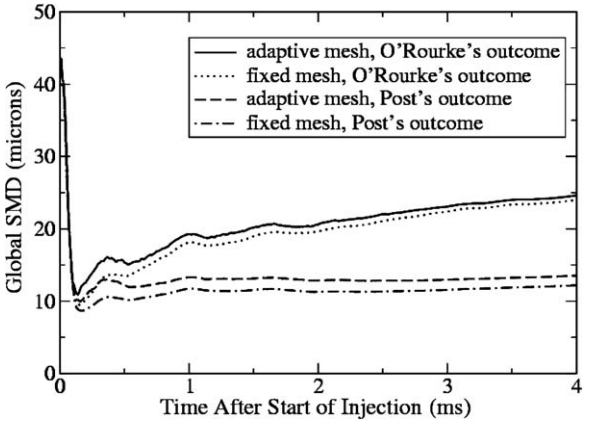

Fig. 18. Effect of the adaptive collision mesh on the predicted global SMD.

the resolution of the adaptive mesh may be comparable to that of the fixed mesh. Collision cell sizes are larger as the spray spreads out. The other reason is that more droplets have undergone collisions, which results in more uniform drop velocities. This makes the collision rate lower because of the decreased relative velocities between the droplets.

It is also noted in Fig. 18 that, when using O'Rourke's model, the predicted global SMD with the two meshes approaches the same value much more quickly than with the composite model. As discussed above, the prediction of the collision incidence tends to be more similar for the two meshes as time advances. Also, more collisions will occur at low Weber number as time goes on. For O'Rourke's outcome model, low Weber number tends to result in permanent coalescence, which constantly changes droplet sizes. So the predicted droplet sizes by the two meshes get close as time progresses. However, bouncing is favored for low Weber number for the composite outcome model, which does not change droplet sizes. Thus the difference between the predicted global SMD by the two meshes is almost constant.

Calculations were also performed for the 40-μm nozzle to assess the effect of the satellite droplet model. The spray tip penetration is not sensitive to the satellite droplet model as shown in Fig. 19. On the other hand, the model has significant effect on the predicted droplet sizes as illustrated in Figs. 20 and 21. The predicted global SMD decreases more than 45% with the satellite droplet model. It is clear that in order to achieve good

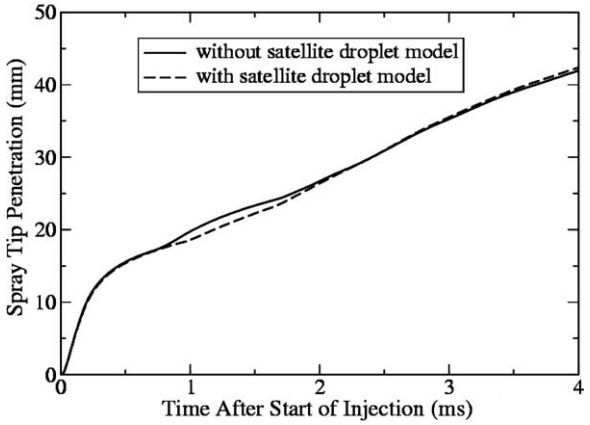

Fig. 19. Effect of the satellite droplet model on the predicted spray tip penetration.

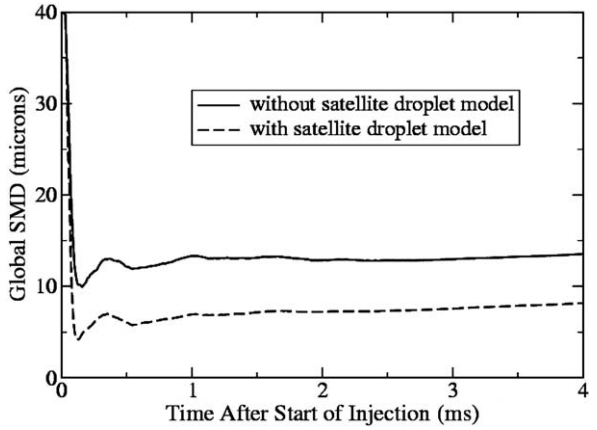

Fig. 20. Effect of the satellite droplet model on the predicted global SMD.

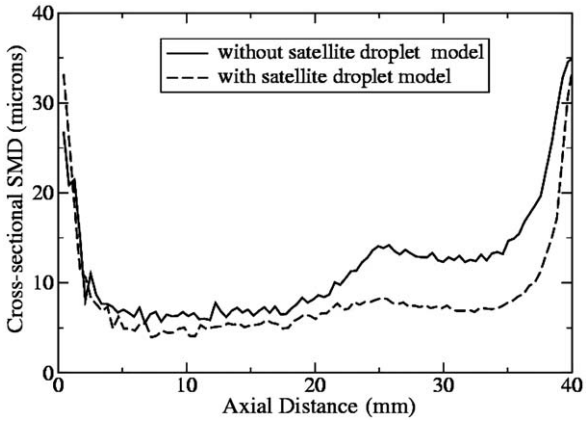

Fig. 21. Effect of the satellite droplet model on the predicted cross-sectional SMD.

agreement with the experimental data, other spray sub-models need to be re-tuned. This conclusion was also reached by Aumann et al. (2002), who evaluated Post and Abraham's collision model.

5. Conclusions

The new collision mesh was shown to be capable of achieving high spatial resolution and at the same time providing accurate statistical representation of collision incidence. The collision mesh does not demonstrate grid artifacts and is applicable to any orifice configuration. The user must employ a large number of parcels in order to achieve good spatial and statistical resolution. Similar to refining the gas phase mesh, the more resources that are available, the better the resolution will be. In the current work, no fewer than 160,000 parcels were used. The numerical parameter that controls the trade-off between spatial and statistical resolution, the partitioning criterion, was investigated. A value of 80 was found to be adequate, though a theoretical analysis suggests that an even lower value could be used.

A phenomenological modification was made to Georjon and Reitz's satellite droplet model that reduced the volume of liquid involved in ligament stretching. The altered model was shown to produce improved agreement with the experimental data. The features of the post-collision drop size distribution, such presence of very small drops, were predicted by the model. The bi-modal drop size distribution of Brenn et al.'s experiment was also captured.

The adaptive collision mesh was also applied to a non-vaporizing high-speed spray, and the predicted results were in good agreement with the experimental data. Due to its higher spatial resolution, the collision mesh was shown to predict higher collision rates and tended to produce larger droplets as compared with the fixed gas phase mesh. It was also shown that the satellite droplet model significantly reduced the predicted droplet sizes. However, in realistic sprays, collision is only partly responsible for the drop size distribution. Many other models are responsible, as well, for the spray prediction. Given the current state of the art of spray modeling, with heavy reliance on empiricism and tuned constants, new collision outcome models should likely be used in concert with re-tuned spray breakup models.

Acknowledgements

This work was funded by Caterpillar Inc. and General Motors Inc. We thank Convergent Thinking LLC for generously sharing their Navier–Stokes solver.

Appendix A

This appendix is devoted to proving that the NTC method can produce the correct average number of collisions with a widely varying sample size. Though this result is shown empirically in the main text, a

mathematical proof may also be of use to the reader. For this proof, we start with a spatially uniform distribution of droplets, so that changing the number of the collision cells changes the sample sizes without altering spatial resolution. The proof initially assumes that the volume of each cell is the same; the oct-tree adaptive resolution is discussed near the end of the Appendix. The number of parcels, N_p, and the volume, $\mathcal{V}$, are fixed. Each parcel represents a stochastically chosen number of droplets denoted as q. The expected number of droplet collisions M_{coll} (not to be confused with parcel collisions) over a short period Δt can be predicted from basic kinetic theory (Schmidt and Rutland, 2000)

$$M_{\text{coll,exact}} = \frac{1}{2}\sum_{i=1}^{N_p} q_i \sum_{j=1}^{N_p} q_j \frac{v_{i,j}\sigma_{i,j}\Delta t}{\mathcal{V}} \tag{A.1}$$

Here, v is the relative velocity and σ is the collision cross-section, defined by (A.2)

$$\sigma_{i,j} = \pi(r_i + r_j)^2 \tag{A.2}$$

We can take an average relative velocity and cross-section over the entire set of $N_p(N_p - 1)/2$ possibilities, excluding the case where $i = j$, and thus the relative velocity is zero. The number of drops per parcel also appears in predicting the number of droplet collisions. Eq. (A.1) can be expressed using this average

$$M_{\text{coll,exact}} = \frac{N_p(N_p - 1)}{2}\frac{\overline{(q^2 v\sigma)}\Delta t}{\mathcal{V}} \tag{A.3}$$

Eq. (A.3) is the exact answer, for which the NTC method is known to give the correct result if the whole volume is treated as one large cell. It remains to be proven that if a domain is subdivided into smaller cells, that the NTC method will continue to predict the correct number of collisions. The primary concern is that with too fine of a mesh, fewer than two parcels may be found in many cells. Collision requires at least two parcels per cell. Hence, if the collision mesh becomes too fine, it is conceivable that the predicted collisions could be artificially suppressed.

The parameter that varies in this proof is the number of collision cells, N_{cells}, into which the volume is divided. The volume of each collision cell is given by (A.4).

$$\mathcal{V}_{cell} = \frac{\mathcal{V}}{N_{cells}} \tag{A.4}$$

Due to random variation in the parcel number density, cells will contain varying number of parcels. We start by examining a collision cell that contains k parcels. Note that unlike the average number of parcels per cell, k must be an integer. If implemented as described in Schmidt and Rutland, the NTC method will sample with replacement a subset of the $k^2/2$ possible parcel pairs in the cell. In the case where the same parcel is sampled twice, the relative velocity is zero. For the other $k(k-1)/2$ possibilities, the collision probability depends on the same average used in Eq. (A.3). When applied to a set of k parcels, the NTC method will predict $M_{coll,k}$ collisions.

$$M_{\text{coll},k} = \frac{k(k-1)}{2}\frac{\overline{(q^2 v\sigma)}\Delta t}{\mathcal{V}} \tag{A.5}$$

Though the distribution of parcels is statistically uniform, chance will dictate that there is a distribution of values of k. This is an example of a Bernoulli experiment, since the location of each parcel is an independent event with two outcomes: a parcel is in the collision cell of interest or it falls into another cell. Hence the probability ρ_k of there being k parcels in a cell is given by the binomial distribution, as shown in (A.6). The value of p, the probability of a given parcel being in the collision cell of interest, is the reciprocal of the number of collision cells

$$\rho_k = \binom{N_p}{k} p^k (1-p)^{N_p - k} \tag{A.6}$$

The expected number of cells with k parcels is the product of ρ_k and the total number of cells, N_{cells}. Thus, the expected number of collisions predicted over the entire domain can be determined from a combination of the expected number of cells with k parcels and the expected number of collisions given k

$$M_{coll} = \sum_{k=0}^{N_p} \rho_k N_{cells} M_{coll,k} \tag{A.7}$$

From here, the number of collisions predicted by the NTC method and the collision mesh can be calculated using only arithmetic. Note that the number of collisions for cells with fewer than two parcels ($k < 2$) is zero, and so the starting limit of the summation can be changed.

$$M_{coll} = \sum_{k=2}^{N_p} \frac{N_p!}{k!(N_p-k)!} p^k (1-p)^{N_p-k} N_{cells} \frac{k(k-1)(\overline{q^2 v\sigma})\Delta t}{2\mathcal{V}_{cell}} \tag{A.8}$$

$$M_{coll} = \frac{N_{cells}(\overline{q^2 v\sigma})\Delta t}{2\mathcal{V}_{cell}} \sum_{k=2}^{N_p} \frac{N_p!}{(k-2)!(N_p-k)!} p^k (1-p)^{N_p-k} \tag{A.9}$$

$$M_{coll} = \frac{N_p \cdot (N_p-1) p^2 N_{cells}(\overline{q^2 v\sigma})\Delta t}{2\mathcal{V}_{cell}} \sum_{k=2}^{N_p} \frac{(N_p-2)!}{(k-2)!(N_p-k)!} p^{k-2} (1-p)^{N_p-k} \tag{A.10}$$

At this point, a change of variable simplifies the summation. The new variable, ℓ, equals k plus two

$$M_{coll} = \frac{N_p \cdot (N_p-1) p^2 N_{cells}(\overline{q^2 v\sigma})\Delta t}{2\mathcal{V}_{cell}} \sum_{\ell=0}^{N_p-2} \frac{(N_p-2)!}{\ell!(N_p-\ell-2)!} p^{\ell} (1-p)^{N_p-\ell-2} \tag{A.11}$$

The ratio of factorials is a standard combinatorial expression and can be re-written using the notation of Eq. (A.12)

$$M_{coll} = \frac{N_p \cdot (N_p-1) p^2 N_{cells}(\overline{q^2 v\sigma})\Delta t}{2\mathcal{V}_{cell}} \sum_{\ell=0}^{N_p-2} \binom{N_p-2}{\ell} p^{\ell} (1-p)^{N_p-2-\ell} \tag{A.12}$$

The argument of the summation represents the probability of ℓ occurrences in $N_p - 2$ trials of a binary event that has an individual probability of p. The limits of the summation include the probabilities of all possible outcomes, presuming there are at least two parcels in total. Hence, the summation is equal to unity. Eq. (A.12) is further simplified by using the fact that p is the reciprocal of the number of cells, giving the final result, Eq. (A.13)

$$M_{coll} = \frac{N_p(N_p-1)}{2} \frac{(\overline{q^2 v\sigma})\Delta t}{\mathcal{V}} \tag{A.13}$$

The result of Eq. (A.13) is independent of the number of cells and the average number of parcels per collision cell. Further, Eq. (A.13) shows the prediction of the NTC method with numerous cells is exactly equal to the correct answer, given in Eq. (A.3). Hence, even with very small sample sizes, the NTC method can produce accurate average answers. For example, numerical tests on a spatially homogenous volume with 25,000 parcels and an average of one parcel per cell (25,000 collision cells) were run. This test is the same as that reported in Fig. 7. The collision mesh was uniform and not recursively adapted. The predicted number of collisions was within 2.5% of the correct answer. This accurate result is despite the fact that 74% of the cells contained zero or one parcel and did not have any collisions at all.

This derivation can be applied to oct-tree adaptive resolution, though one would not actually need adaptive resolution on a spatially homogenous distribution of parcels. For oct-tree adaptation, consider the global volume $\mathcal{V}$, as used above, to represent the unrefined cell. The above proof shows that dividing a volume into eight

cells does not change the predicted number of collisions for a spatially homogenous parcel distribution *so long as the number of parcels in the parent cell is greater than or equal to two*. This restriction of two or more parcels comes from the assumption used in going from Eqs. (A.12) and (A.13). We noted that the summation is equal to unity, since it represents the sum of the probabilities of all outcomes of a Bernoulli trial. However, if N_p is less than two, then the set of outcomes described by Eq. (A.12) is the empty set. The summation effectively equals zero for one or fewer parcels. For more than one parcel in the parent cell, Eq. (A.13) is valid and refinement creates no bias error. Since this conclusion about dividing a cell into eight sub-cells can be applied recursively, the general statement is proven: the oct-tree adaptation produces, on average, the correct answer so long as cells with fewer than two cells are not refined.

References

Abraham, J., 1997. What is adequate resolution in the numerical computations of transient jets?, SAE Technical Paper 970051.

Alexander, F., Garcia, A., 1997. The direct simulation Monte Carlo method. Comput. Phys. 11, 588–593.

Amsden, A.A., O'Rourke, P.J., Butler, T.D., 1989. KIVA-II A computer program for chemically reactive flows with sprays. Los Alamos National Laboratory, LA-11560-MS.

Aneja, R., Abraham, J., 1998. How far does the liquid penetrate in a diesel engine: computed results vs. measurements? Combust. Sci. Technol. 138, 233–255.

Arai, M., Saito, M., 1999. Atomization characteristics of jet-to-jet and spray-to-spray impingement systems. Atomization Sprays 9, 399–417.

Are, M., Hou, S., Schmidt, D.P., 2005. Second order spatial accuracy in Lagrangian–Eulerian spray calculations. Numer. Heat Transfer 48, 25–44.

Ashgriz, N., Poo, J.Y., 1990. Coalescence and separation in binary collisions of liquid drops. J. Fluid Mech. 221, 183–204.

Aumann, R., McCracken, M., Abraham, J., 2002. An evaluation of a composite model for predicting drop–drop collision outcomes in multidimensional spray computations. SAE Paper 2002-01-0943.

Baik, S., Blanchard, J.P., Corradini, M.L., 2003. Development of micro-diesel injector nozzles via MEMS technology and effects on spray characteristics. Atomization Sprays 13, 443–474.

Bartlett, M.S., 1963. Statistical estimation of density functions. Sankhyā, Ser. A 25, 245–254.

Bird, G.A., 1989. Perception of numerical methods in rarefied gas dynamics. Prog. Astronaut. Aeronaut. 118, 211.

Brazier-Smith, P., Jennings, S., Latham, J., 1971. The interaction of falling rain drops: coalescence. Proc. Roy. Soc. London A326, 393–408.

Brenn, G., Kalenderski, S., Ivanov, I., 1997. Investigation of the stochastic collisions of drops produced by Rayleigh breakup of two laminar jets. Phys. Fluids 9, 349–364.

Estrade, J.-P., Carentz, H., Lavergne, G., Biscos, Y., 1999. Experimental investigation of dynamic binary collision of ethanol droplets—a model for droplet coalescence and bouncing. Int. J. Heat Fluid Flow 20, 486–491.

Garcia, A.L., 2000. Numerical Methods for Physics. Prentice-Hall, Englewood Cliffs, NJ.

Gavaises, M., Theodorakakos, A., Bergeles, G., Brenn, G., 1996. Evaluation of the effect of droplet collision on spray mixing. Proc. Inst. Mech. Eng. 210, 465–475.

Georjon, T.L., Reitz, R.D., 1999. A drop-shattering collision model for multidimensional spray computations. Atomization Sprays 9, 231–245.

Hieber, S.E., 2001. An investigation of the mesh dependence of the stochastic discrete droplet model applied to dense liquid sprays. Master Thesis, Department of Mathematical Science, Michigan Technological University.

Hou, S., Schmidt, D.P., 2004. Modeling droplet collision with adaptive meshing and updated outcomes. SAE Congress, Detroit, Paper 2004-01-0533.

Hung, C.C., 1998. Insights into droplet behavior within high pressure diesel sprays. Ph.D. Dissertation, Department of Mechanical Engineering, University of Wisconsin-Madison.

Issa, R.I., 1985. Solution of the implicitly discretised fluid flow equations by operator-splitting. J. Comput. Phys. 62, 45–60.

Jiang, Y., Umemura, A., Law, C.K., 1992. An experimental investigation on the collision behavior of hydrocarbon droplets. J. Fluid Mech. 234, 171–190.

MacInnes, J., Bracco, F.V., 1991. Comparisons of deterministic and stochastic computations of drop collisions in dense sprays. Numer. Approach. Combust. Model. 135, 615–642.

Nordin, N., 2000. Complex Chemistry Modeling of Diesel Spray Combustion. Ph.D. Dissertation, Chalmers University of Technology.

Orme, M., 1997. Experiments on droplet collisions, bounce, coalescence and disruption. Prog. Energy Combust. Sci. 23, 65–79.

O'Rourke, P.J., 1981. Collective drop effects on vaporizing liquid sprays. Ph.D. Dissertation, Department of Mechanical and Aerospace Engineering, Princeton University.

O'Rourke, P.J., Amsden, A.A., 1987. The TAB method of numerical calculation of spray droplet breakup. SAE Paper 872089.

Park, J.H., Baek, S.W., Kang, S.J., Yu, M.J., 2002. Analysis of thermal slip in oscillating rarefied flow using DSMC. Numer. Heat Transfer, Part A 42, 647–659.

Post, S.L., Abraham, J., 2002a. Modeling collision among drops with a non-uniform spatial distribution. ILASS Americas. In: 15th Annual Conference on Liquid Atomization and Spray Systems, Madison, Wisconsin.

Post, S.L., Abraham, J., 2002b. Modeling the outcome of drop–drop collisions in diesel sprays. Int. J. Multiphas. Flow 28, 997–1019.
Qian, J., Law, C.K., 1997. Regimes of coalescence and separation in droplet collision. J. Fluid Mech. 331, 59–80.
Reitz, R.D., 1987. Modeling atomization processes in high-speed vaporizing sprays. Atomization Sprays 3, 309–337.
Reitz, R.D., Diwakar, R., 1987. Structure of high-pressure fuel sprays. SAE Paper 870598, 492–509.
Schmidt, D.P., Rutland, C.J., 2000. A new droplet collision algorithm. J. Comput. Phys. 164, 62–80.
Schmidt, D.P., Rutland, C.J., 2001. Reducing grid dependency in droplet collision calculations. Fall ASME ICE Meeting, Argonne National Laboratory.
Subramaniam, S., 2001. Statistical modeling of sprays using the droplet distribution function. Phys. Fluids 13.
Zhou, Q., Leschziner, M.A., 1991. A Lagrangian particle dispersion model based on a time-correlated stochastic approach. ASME FED-vol. 121, Gas–Solid Flows, pp. 255–260.